AAPT PHYSICS EDUCATION | AMERICAN JOURNAL of PHYSICS

Low-cost diffuse optical tomography for the classroom

Taisuke Minagawa, Peyman Zirak, Udo M. Weigel, Anna K. Kristoffersen, Nicolas Mateos et al.

Citation: Am. J. Phys. **80**, 876 (2012); doi: 10.1119/1.4739924
View online: http://dx.doi.org/10.1119/1.4739924
View Table of Contents: http://ajp.aapt.org/resource/1/AJPIAS/v80/i10
Published by the American Association of Physics Teachers

Related Articles

Rounding off the cow: Challenges and successes in an interdisciplinary physics course for life science students
Am. J. Phys. 80, 913 (2012)

Resource Letter BSSMF-1: Biological Sensing of Static Magnetic Fields
Am. J. Phys. 80, 851 (2012)

Plant Physics
Am. J. Phys. 80, 842 (2012)

Dual X-ray absorptiometry
Am. J. Phys. 80, 621 (2012)

Resource Letter EIRLD-2: Effects of Ionizing Radiation at Low Doses
Am. J. Phys. 80, 274 (2012)

Additional information on Am. J. Phys.

Journal Homepage: http://ajp.aapt.org/
Journal Information: http://ajp.aapt.org/about/about_the_journal
Top downloads: http://ajp.aapt.org/most_downloaded
Information for Authors: http://ajp.dickinson.edu/Contributors/contGenInfo.html

ADVERTISEMENT

Low-cost diffuse optical tomography for the classroom

Taisuke Minagawa, Peyman Zirak, Udo M. Weigel, Anna K. Kristoffersen, Nicolas Mateos, Alejandra Valencia, and Turgut Durduran
ICFO—Institut de Ciències Fotòniques, Mediterranean Technology Park, 08860 Castelldefels (Barcelona), Spain

(Received 9 February 2012; accepted 12 July 2012)

Diffuse optical tomography (DOT) is an emerging imaging modality with potential applications in oncology, neurology, and other clinical areas. It allows the non-invasive probing of the tissue function using relatively inexpensive and safe instrumentation. An educational laboratory setup of a DOT system could be used to demonstrate how photons propagate through tissues, basics of medical tomography, and the concepts of multiple scattering and absorption. Here, we report a DOT setup that could be introduced to the advanced undergraduate or early graduate curriculum using inexpensive and readily available tools. The basis of the system is the LEGO Mindstorms NXT platform which controls the light sources, the detectors (photo-diodes), a mechanical 2D scanning platform, and the data acquisition. A basic tomographic reconstruction is implemented in standard numerical software, and 3D images are reconstructed. The concept was tested and developed in an educational environment that involved a high-school student and a group of post-doctoral fellows.
[http://dx.doi.org/10.1119/1.4739924]

I. INTRODUCTION

We recognize visible light and light-based tools as the fundamental components of vision and imaging. However, when it comes to medical imaging, and, in particular, non-invasive imaging of deep tissues, visible light is rarely used because tissues are not transparent in visible frequencies. Non-invasive medical imaging of deep tissues is, therefore, normally associated with other parts of the electromagnetic spectrum such as x-rays.

In 1929, a report[1] was published which employed light to "see" tumors lying deep in the female breast. This technique was termed "transillumination" or "diaphanography," and it was utilized until the mid-1980s when it became evident that the lack of a physical model severely limited the ability to make from it a quantitative analysis. The early 1990s saw the emergence of such a model and the full appreciation of the role of the physics of photon propagation in tissues. This led to the development of biomedical diffuse optical tomography (DOT). The term "diffuse optics" became widely accepted since light propagation over long distances in tissues is well approximated as a diffusive process.[2] This recognition has provided the necessary physical model to quantitatively separate tissue scattering from tissue absorption, and to accurately incorporate the influence of boundaries and heterogeneities. Thus, it paved the way for *quantitative* measurements of diffuse optics. DOT is now utilized in testing a variety of potential clinical applications in oncology, neurology, and other areas where tissue oxygen metabolism and hemodynamics play an important role.[3]

From an educational viewpoint, as the field of biomedical optics is advancing and the technology is getting mature, courses where the field is treated have been introduced across the world in a variety of disciplines ranging from physics to biomedical engineering and radiology. Such courses are often presented in a highly theoretical manner (see, for example, two recently published textbooks[4,5]), in a semester-long course or as part of a survey class, where several lectures and some demonstrations are presented to the students. Generally, any biomedical optics course includes a brief introduction to diffuse optics.

In this paper, we present a demonstration of a DOT setup using off-the-shelf, inexpensive components. The experimental setup can be used as a tool to introduce physical and biomedical concepts to physics and life science majors in a biomedical optics class. LEGO Mindstorms NXT components[6] are used as the basis for controlling the light sources, acquiring data from a detector, controlling a two-dimensional mechanical scanner, and handling the data. The use of LEGO components and its educational robotics platform make the setup inexpensive yet versatile and attractive for the students. The setup that we report here was developed in a summer project, where a final year high-school student spent a month in our laboratory with a group of post-doctoral fellows studying the basics of photon diffusion and designing and implementing the system. It was then presented in a medical optics class.

II. PHOTON DIFFUSION IN TISSUES

Diffuse optics in bio-medicine uses light sources and detectors in the red/near-infrared wavelength regime ($\lambda = 600 - 1000$ nm). This is the "physiological window" wherein the overall absorption due to main tissue absorbers such as deoxy and oxy-hemoglobin and water is relatively small. This in turn implies that losses are less, and light can penetrate tissues significantly deeper than visible and further-infrared light (see Fig. 1). This absorption can be described by an absorption length that is roughly 100 mm, whose reciprocal, the absorption coefficient, is denoted $\mu_a(\lambda)$.[7]

In addition to the absorption process, photon propagation in tissues also involves multiple scattering. The characteristic "scattering length" is the typical distance traveled by photons before they scatter, which is roughly $1-100$ μm. Since the scattering process is also highly anisotropic, the subsequent formalism uses a longer "random walk step" ($\sim$ 1 mm), which corresponds to the typical distance traveled by photons

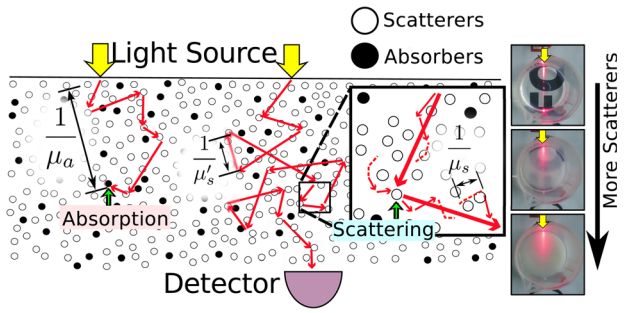

Fig. 1. (Color online) Schematic view of the absorption and scattering processes. Photons are scattered by scatterers in a length scale of $1/\mu_s$, and the photon direction gets randomized in $1/\mu_s'$. There is also a probability that photons are absorbed by absorbers in a length scale of $1/\mu_a$ before reaching to a detector. Normally, $\mu_s' \gg \mu_a$, and scattering events dominate the diffusion process. The images at right show actual light propagation with different scatterer concentrations.

before their directions are randomized. The reciprocal of this length is the reduced scattering coefficient, $\mu_s'(\lambda)$.[7]

Comparing these two length scales, one can see that the propagation of photons at these wavelengths is dominated by multiple scattering. In other words, their propagation could be approximated as a diffusive process. A conceptual introduction to photon diffusion is available in a tutorial format in Ref. 7. A photon diffusion model could be used to decouple the wavelength and position dependent absorption and scattering coefficients from each other.[7] As will be shown in the discussion below, this also implies that tomography with diffuse light is more complex than commonly available computed tomography.[8,9] In general, the formalism starts from the radiative transport equation for photons and employs a variety of assumptions to reach a time-dependent photon diffusion equation. To learn more about the details of the formalism, we refer our readers to various recent reviews.[3,9]

A. Photon diffusion equation

In order to introduce DOT in the classroom, it is appropriate, and cost- and time-effective, to utilize a continuous wave (CW) light source, which delivers constant light into the system. As shown in the Fig. 2, we utilize a CW source located below the origin pointing at the $-z$ direction ($z = z_0$)

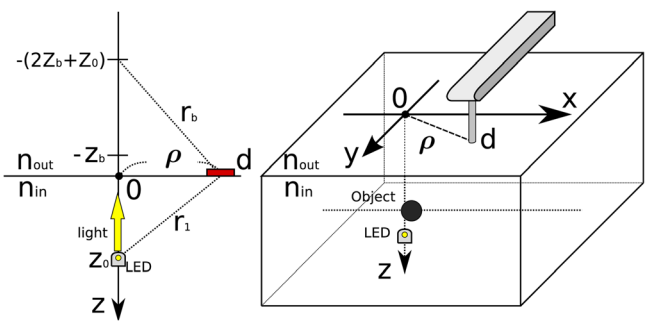

Fig. 2. (Color online) A schematic view of the semi-infinite model (left) and the experimental setup (right). The light source (LED, $z = 5.5$ cm) is located deep inside the turbid medium. The detector (photo-diode, $z = 0$ cm) scans at the interface between the air (refractive index n_{out}) and the turbid medium (refractive index n_{in}). An image source in the air side ($z = -(2z_b + z_0)$) is used to calculate the fluence analytically. Distances (r) are measured from sources (both real and image) to detectors. The planar distance is defined by $\rho = \sqrt{x^2 + y^2}$. The bottom boundary of the container is located at $z = 8.3$ cm.

which is considered as a point source. Photons take randomized paths ("random walk") due to the scattering events and are detected at the surface of medium ($z = 0$). We describe the light intensity using the photon fluence $\Phi(r)$, with units of joule per centimeter square (Fig. 1). Starting from the radiative transfer equation and working in the diffusion limit ($\mu_s' \gg \mu_a$), one can show that the fluence is described by the diffusion equation[5]

$$(\nabla^2 - \mu_{\text{eff}}^2)\Phi(r) = -\frac{S}{D}\delta(r), \tag{1}$$

where $\mu_{\text{eff}} = \sqrt{3\mu_a \cdot (\mu_a + \mu_s')} \approx \sqrt{3\mu_a\mu_s'}$ is an effective attenuation coefficient, $D = 1/\mu_{\text{eff}}$, S is the constant strength of the light source, and $r = |\mathbf{r}^d - \mathbf{r}^s|$ is the separation distance between the source (at $\mathbf{r}^s$) and the detector (at $\mathbf{r}^d$). This equation has different solutions depending on the boundary conditions. The simplest case that could be solved using a standard Green's function approach is an infinite, i.e., no boundaries, homogeneous medium where $\Phi(r) = S\exp(-\mu_{\text{eff}}r)/(4\pi Dr)$. This equation shows a damped, spherically symmetric, steady-state diffusion of light from a point source of power S. This scenario seems fictitious, but since the photon fluence decays exponentially, even reasonably small turbid media such as a 10 liter fish-tank could be well approximated by this equation.

A more realistic model is a semi-infinite homogeneous medium which assumes an infinite, planar interface between the turbid medium (tissue) and air (Fig. 2). This is one of the most commonly used models in DOT.[3,7] The Green's function solution for this geometry can be obtained using an image source at $z = -(2z_b + z_0)$, assuming that the fluence falls to zero at an extrapolated plane on the air side at $-z_b$. The fluence for the semi-infinite medium is therefore

$$\Phi(\vec{r}) = \frac{S}{4\pi D}\left[\frac{\exp(-\mu_{\text{eff}}r_1)}{r_1} - \frac{\exp(-\mu_{\text{eff}}r_b)}{r_b}\right], \tag{2}$$

where r_1 is the distance between the detector (in our experiment at $z = 0$) and the point source (in our experiment at $z = 5.5$ cm) in the turbid medium, while r_b is the distance between the detector and the image source. Here, $z_b = 2z_0(1 + R_{\text{eff}})/3(1 - R_{\text{eff}})$, and $R_{\text{eff}} \approx -1.440n^{-2} + 0.710n^{-1} + 0.668 + 0.0636n$ is the effective reflection coefficient, which is a commonly used approximate value.[5] The parameter $n = n_{\text{in}}/n_{\text{out}}$ is the ratio of the indices of refraction inside and outside the medium.

This semi-infinite model can either be fitted exactly, or in the case of large source–detector separations, it can be approximated by a linear equation as[3]

$$\ln\left(r^2\Phi(r)\right) = -\mu_{\text{eff}} \cdot r + \text{const.} \tag{3}$$

This form implies that the measured intensity by a detector is proportional to the fluence, and the logarithmic decay of the intensity with increasing source–detector separation can be approximated by a line with a slope $-\mu_{\text{eff}}$. This slope can be fitted and used to characterize the turbid medium.

B. 3D tomography with diffusing photons

Tomography has entered the medical imaging literature via x-ray computed tomography, which allows 3D volumetric

imaging of the internal organs by utilizing an image reconstruction based on the inverse problem of the data acquired at multiple views from the outside. Unlike 3D rendering of the surfaces, this implies a truly 3D reconstruction of the whole volume, where internal structures that are not visible from the outside are resolved.[8]

The first step in constructing the model needed for tomographic image reconstruction is to estimate the volumes that are probed by the imaging modality. In DOT, this would be the estimation of the visiting probability of the photons through each volume element ("voxel") in the probed tissue volume. This is calculated using the Green's functions described above and leads to the "banana patterns" (Fig. 3) for each source–detector pair, which is a term commonly used in diffuse optics.[10]

The simplest model assumes a linear dependence between a set of these functions for each source–detector pair and all volume elements and the properties of the probed volume to estimate the measured intensity by that detector. Furthermore, if a perturbative approach is taken and the data from a homogeneous medium is compared to that from a small heterogeneity in the probe volume, i.e., within the "banana pattern," then the perturbation of the measurements can be estimated using this model. The idea of DOT within this simplification is that by knowing the difference between photon propagation with and without the perturbation by the heterogeneity, one can estimate the properties of the heterogeneity (optical properties, physical size and location) based on mathematical models.

The process is illustrated in Fig. 3 and below we outline the mathematical formalism. If we assume that the entire system is homogeneous except for a small inhomogeneity of increased absorption $\delta\mu_a(\mathbf{r})$, that is, $\mu_a \rightarrow \mu_a + \delta\mu_a(\mathbf{r})$, where μ_a is for the background homogeneous material, then in the Born approximation,[8] the perturbation of the fluence (denoted "sc" for "scattered fluence") is given by

$$\Phi_{\mathrm{sc}}(\mathbf{r}^d - \mathbf{r}^s) = \Phi(\mathbf{r}^d - \mathbf{r}^s) - \Phi'(\mathbf{r}^d - \mathbf{r}^s). \tag{4}$$

Here $\Phi(\mathbf{r}^d - \mathbf{r}^s)$ is the fluence within the semi-infinite medium without the perturbation, and $\Phi'(\mathbf{r}^d - \mathbf{r}^s)$ is the fluence with the perturbation. By inserting this expression into Eq. (1) and discretizing it into N voxels in space, we obtain a matrix equation of the form $[\Phi^{\mathrm{sc}}] = [J] \cdot [\delta\mu_a]$, whose elements are given by[3]

$$\Phi_{\mathrm{sc}}(\mathbf{r}_k^d - \mathbf{r}_i^s) = A\sum_{j=1}^{N} G(\mathbf{r}_k^d - \mathbf{r}_j)\,\Phi(\mathbf{r}_j - \mathbf{r}_i^s)\,\delta\mu_a(\mathbf{r}_j). \tag{5}$$

This equation relates all the measurements (the ith source position $\mathbf{r}_i^s$ and the kth detector position $\mathbf{r}_k^d$) to both the background and perturbed optical properties for all voxel positions, $\mathbf{r}_j$, in the probed volume. Here, $A = h^3/D$ is a constant with a voxel volume of h^3, and $G(\mathbf{r}) = D\Phi(\mathbf{r})/S$ is the Green's function solution. In Fig. 3, we have N_s sources and N_d detectors, and the Jacobian $[J]$ is a matrix of dimension $(N_d \cdot N_s) \times N$.

The goal is to measure $[\Phi^{\mathrm{sc}}]$, calculate $[J]$, and then invert this system to obtain $[\delta\mu_a]$, which is a 3D image of the hidden perturbation deep inside the turbid medium, i.e., tissue.

However, this inversion is a complex process.[8,9] One implementation solves the problem in the form

$$[\delta\mu_a] = \left([J]^T[J] + [C(\mathbf{r}_j)]^T[C(\mathbf{r}_j)]\right)^{-1}[J]^T[\Phi^{\mathrm{sc}}]. \tag{6}$$

Here the superscripts "T" and "-1" denote matrix transpose and inverse, respectively. The product $[J]^T[J]$ is calculated to create a square matrix that can be inverted, but due to the nature of the DOT problem, it is generally a singular matrix and the whole problem is ill-posed. To reduce imaging artifacts due to this fact, we add a regularization matrix,

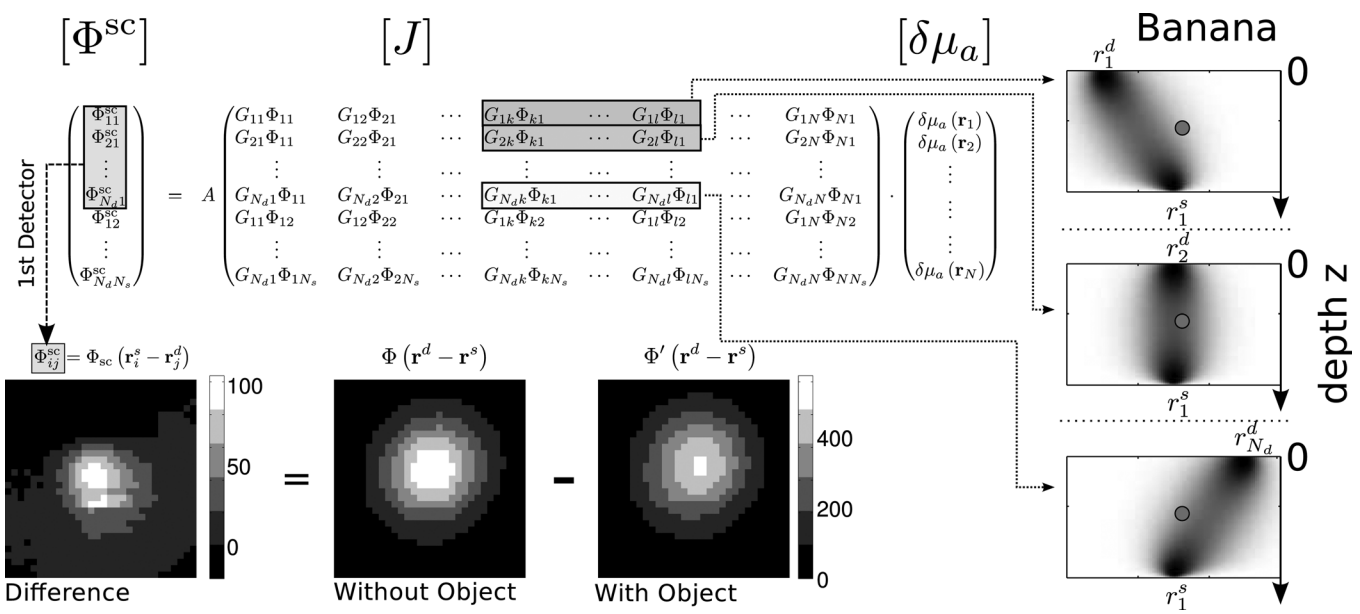

Fig. 3. A schematic view of Eq. (5), where $\Phi_{ij}^{\mathrm{sc}} = \Phi_{\mathrm{sc}}(\mathbf{r}_i^s - \mathbf{r}_j^d)$, $G_{ij} = G(\mathbf{r}_i^d - \mathbf{r}_j)$ and $\Phi_{ji} = \Phi(\mathbf{r}_j - \mathbf{r}_i^s)$. One of the elements of $[\Phi^{\mathrm{sc}}]$, Φ_{n1}^{sc}, is the measured fluence difference between with and without the small black sphere for a source ($\mathbf{r}_1^s$) and detector ($\mathbf{r}_n^d$). In the Jacobian matrix $[J]$, the row elements (k to l) represent slices of the photon visiting probabilities ("banana patterns" or shaded regions) as shown at right. We show bananas for different detector positions for a fixed source at r_1^s. The location of the heterogeneity is denoted by the small circle. For a given source–detector pair, the perturbation due to the presence of the object is dependent on the overlap of the banana pattern and the object.

$[C(\mathbf{r}_j)]^T[C(\mathbf{r}_j)]$. Effectively, this matrix reduces high spatial frequency noise at the cost of worsened spatial resolution. The matrix $[C(\mathbf{r}_j)]$ has the same dimension as Jacobian $[J]$, and each element has a value of $l_c[1+1000\exp(2z_j/h-1)]$, where $h=8.8$ cm, the depth of the turbid medium in our container, and z_j is the z coordinate of r_j for the corresponding Jacobian element (Eq. (5)). We have voxelized the z direction into 12 elements and used an optimized regularization value of $l_c=1.9\times10^{-6}$ obtained from "L-curve" analysis.[3,9] Regularization of this sort can also be considered as a theoretical knob that could be tuned as a compromise between image noise, spatial resolution, and system stability. It is beyond the scope of this work to enter into a detailed discussion of these inverse problems.[11]

III. EXPERIMENTAL REALIZATION

We started by defining the experimental geometry. A semi-infinite turbid medium was chosen to be the basis of our system with three source positions embedded deeply into the medium and a grid of detector positions that are achieved by mechanically scanning a photo-diode in two dimensions. Two sets of data were acquired for each experiment: one with a homogeneous medium and another with a small heterogeneity present. A small (diameter 0.3 cm) plastic black sphere was chosen to represent an infinitesimally small object with an infinite contrast, i.e., a heterogeneity that is a "delta-function" which could be used to measure the point-spread function (PSF) of the tomographic system. The PSF describes the broadening due to limited spatial resolution, defined by its full width at half maximum. The set-up is illustrated in Fig. 2.

Our goal was to construct a set-up that could be understood at an advanced undergraduate level using low-cost and readily available materials. LEGO Mindstorms NXT (NXT) was chosen as the basis of the set-up since there are plenty of examples that are publicly available. This suggests that it is possible to handle both the mechanical needs (mainly the two-dimensional scanning) and the opto-electronic needs (acquiring data from a photo-diode) of the proposed set-up relatively easily. Furthermore, NXT comes with easy-to-use yet versatile and powerful software (NXT-G), which introduces the concepts of instrument control and data acquisition to the students without the need to learn a complex programming language. Another benefit that we soon realized was that the LEGO pieces are constructed with a sub-millimeter accuracy between their studs which allowed us to utilize a simple yet effective way of controlling and measuring distances such as the source–detector separation. The design is illustrated in Fig. 2.

The next step was to choose the light sources and detectors. There are a variety of light sensors and light sources available from LEGO and from third-party sources, however, their opto-electronic properties were not well defined so we have opted to utilize a readily available yet well-documented photodiode (FDS100, Thorlabs, Germany[13]) and a red (631 nm) LED (LED631E, Thorlabs, Germany). Different wavelengths and multiple detectors can easily be used in the future.

The LEGO NXT kit comes with a micro-controller unit that has some analog-to-digital conversion and digital input/output capabilities, but again the analogue-to-digital (A/D) conversion was not well documented and it would have required that we construct a special circuit to interface the photo-diode with this system. A third-party prototype board (NPS1055, HiTechnic, NY, USA[14]) was readily available which has a 3.3 V analog input that is digitized (10-bit) and is interfaced to the main NXT micro-controller. It comes with a small library that can be used with the NXT-G language.

A small circuit was built on a standard electronics breadboard to power ($\sim$8.0 V and $\sim$0.03 A) the LED in series with a 150 Ω resistor. NXT has a capability of powering an LED, but we have used a standard external power supply to stabilize the output of a source LED. A noise filter and an output resistor (100 kΩ) formed the photodiode circuit. In order to make use of the full 10-bit range of the A/D converter, we have also made an appropriate amplifier ($\times$11 gain) so that the maximum measured light intensity at the shortest source–detector separation can be adjusted to be around $2^{10}=1024$. The dark current of the photodiode and the amplifier combination was measured to be under the 10-bit voltage resolution, i.e., it was recorded as zero.

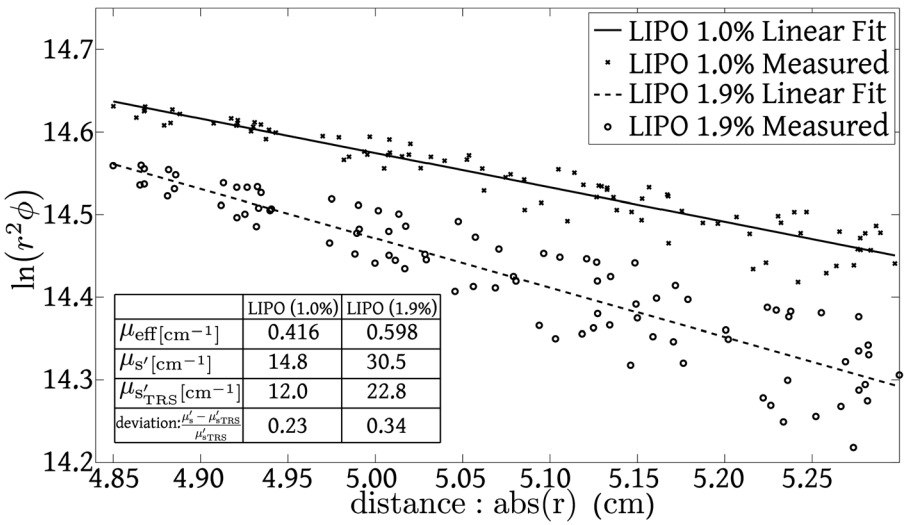

Fig. 4. Data from homogeneous, semi-infinite media (dots) and the fitted lines from the semi-infinite model (Eq. (3), lines) for different Lipofundina concentrations. The agreement between the experiment and the theoretical model is evident. Inset: A summary of measurements for the LEGO and TRS setups.

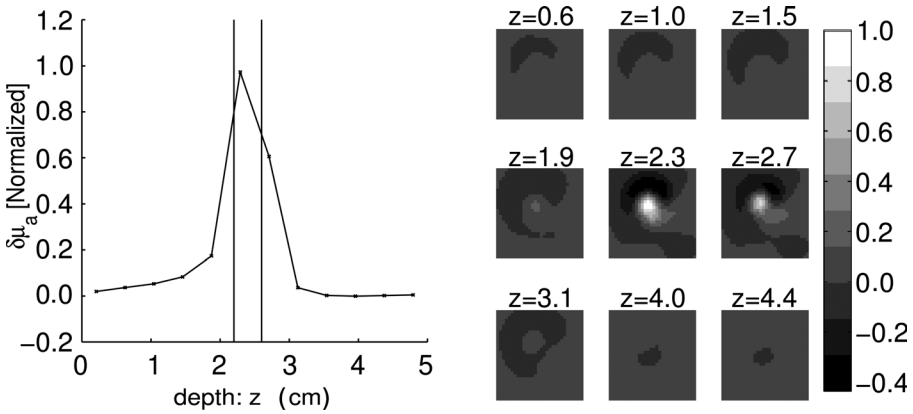

Fig. 5. Left: Calculated and normalized $\delta\mu_a$ along the z axis shows an estimate of the PSF. The two vertical bars indicate the physical size of the black sphere. Right: Slices of $\delta\mu_a$ images along the z direction.

A plastic rectangular container ($35 \times 20 \times 13$ cm) was filled with water mixed with a different concentration of scatterers (Lipofundina, LIPO, BBraun, Spain[15]) to create a turbid medium simulating photon diffusion in tissue. Both the photodiode and the LED were water-sealed with a silicone sealant. The LED light source was placed deep into the turbid medium at $z_0 = 5.5$ cm and the diffuse light was detected by the photo-diode ($z_d = 0$ cm cm) that is scanned on the surface with small steps ($d_x = 0.42 \pm 0.03$ and $d_y = 0.40 \pm 0.02$ cm) in a square grid. We have carefully chosen and calibrated the driving motor power and the translational direction to achieve a sub-millimeter accuracy. Furthermore, the scanning directions are always kept forward. At the end of a forward scan, the detector is moved backward to Δl behind of the origin, then a forward motion is applied to move the detector to the origin to minimize the backlash. The computer code for this motion is provided in the online supplementary material.[12] The fluence was recorded 100 times at each position with a 10 ms averaging. The origin was defined to be vertically above the first source position, which was determined based on the assumption that the photon fluence is peaked at that point, and was adjusted by repeated small step size scans.

A. Determination of the bulk optical properties

The first step is to characterize the optical properties of the turbid medium, which are needed to calculate the Jacobian. Since continuous-wave measures make the separation of the μ_a and μ_s' difficult, we have elected to rely on the literature for the absorption coefficient of the water, and to measure the scattering coefficient only by fitting the effective attenuation coefficient, μ_{eff}, using Eq. (3). The phantom was prepared using standard methods where LIPO 20% was used as the scattering medium with two concentrations (1.0% and 1.9%). We have evaluated 30×31 measurements along x and y directions with respect to the source to fit for μ_{eff} as summarized in an inset of Fig. 4. Furthermore, we have utilized a time-resolved spectroscopy device (TRS) to compare with our results. However, since TRS did not have the correct wavelengths, the values at 631 nm were obtained by extrapolation. Overall, our measurements deviate by 23%–34% from the TRS estimates. The deviations may be due to mechanical errors in our system or to the extrapolation procedure. In the future, we can overcome this by utilizing an LED at another wavelength and/or by utilizing a better-characterized phantom. However, for this project, the goal was to introduce the basics at a low cost and we believe this accuracy is reasonable.

B. 3D tomography

To test the tomographic image reconstruction, we have utilized a small black sphere (diameter 0.3 cm) which was fixed using a transparent fishing-line (diameter 0.035 cm) at $z = 2.6$ cm as shown in Fig. 2. This is a standard way of testing a tomographic system.[9,11] The sphere was located just above but slightly off center from the source and for the reference measurements was removed by pulling the string across a LEGO pulley. This allows us to try to account for the effects of the fishing line in the reference measurement.

Three source positions ($x_s = -0.4$, 0, and 0.4 cm) were scanned to improve our ability to resolve in 3D (Fig. 3), and six surface scans were recorded (three scans for each source with and without the object). We constructed $[\Phi^{sc}]$ as a $30 \times 31 \times 3 = 2790$ row vector. The Jacobian was constructed for each volume element of $0.42 \times 0.40 \times 0.42$ cm^3. Representative panels are shown in Fig. 3 to illustrate each of the components that went into the reconstruction.

Figure 5 (right) shows slices from the detector plane down to the source plane. The object is well localized between $z = 2.3$ cm and $z = 2.7$ cm and is clearly broadened compared to its physical volume. Figure 5 (left) shows a line through the observed object center which indicates the PSF of the system compared to the vertical bars (true object size). In the right panel, the color bar is normalized to 1 at the maximum since a black object does not have a measurable μ_a. Various artifacts are also visible, which are commonly observed in DOT images and may be attributed to small errors in mechanical scanning, signal-to-noise ratio, and to the singular and ill-posed nature of the problem. The regularization parameter could be further fine-tuned to reduce the artifacts and explore its effects on the spatial resolution.

IV. CONCLUSIONS

We have described a LEGO-controlled tomographic scanner to introduce diffuse optical tomography to the classroom. The total cost of the system was approximately 400 Euros. A recent high-school graduate (Nicholas Mateos) spent one summer month to design, construct, and utilize the system. At each step, the student's feedback was utilized to determine

the level of scientific and technological knowledge that is necessary to replicate the project in its final form. The data fidelity was sufficient to estimate the effective attenuation coefficient of the medium, which was in reasonable agreement with a state-of-the-art time-resolved spectroscopy device. A tomographic data set was acquired and reconstructed utilizing a small object with a large perturbation to study the point-spread function of the system and to introduce the student to the concept of regularization in tomographic image reconstruction. The system can be further optimized, expanded, and utilized either as a classroom demonstration or a project for a small team to build from scratch.

We provide an instructional video and the NXT-G codes as supplementary materials.[12] The forward and inverse calculations were done in MATLAB and are available on request to course instructors. We suggest that the programming is included as part of the coursework.

ACKNOWLEDGMENTS

The authors acknowledge support from the Joves i Ciència de Catalunya[16] program funded by Catalunya Caixa and Fundació Cellex Barcelona.

[1]M. Cutler, "Transillumination of the breast," Surg. Gynecol. Obstet. **48**, 721–727 (1929).
[2]A. G. Yodh and B. Chance, "Spectroscopy and imaging with diffusing light," Phys. Today **48**(3), 34–40 (1995).
[3]T. Durduran, R. Choe, W. Baker, and A. G. Yodh, "Diffuse optics for tissue monitoring and tomography," Rep. Prog. Phys. **73**(7), 076701–076744 (2010).
[4]F. Martelli, S. D. Bianco, A. Ismaelli, and G. Zaccanti, *Light Propagation through Biological Tissue and Other Diffusive Media: Theory, Solutions, and Software* (SPIE Publications, Bellingham, Washington, 2009).
[5]L. V. Wang and H. I. Wu, *Biomedical Optics: Principles and Imaging*, 1st ed. (Wiley-Interscience, Hoboken, New Jersey, 2007).
[6]LEGO homepage for educational purposes, <http://education.lego.com/>, accessed April 2012.
[7]S. L. Jacques and B. W. Pogue, "Tutorial on diffuse light transport," J. Biomed. Opt. **13**(4), 041302 (2008).
[8]A. C. Kak and M. Slaney, *Principles of Computerized Tomographic Imaging* (IEEE Service Center, Piscataway, NJ, 1988).
[9]S. R. Arridge and J. C. Schotland, "Optical tomography: Forward and inverse problems," Inverse Probl. **25**(12), 123010 (2009).
[10]B. W. Pogue, S. C. Davis, X. Song, B. A. Brooksby, H. Dehghani, and K. D. Paulsen, "Image analysis methods for diffuse optical tomography," J. Biomed. Opt. **11**, 033001 (2006).
[11]J. P. Culver, R. Choe, M. J. Holboke, L. Zubkov, T. Durduran, A. Slemp, V. Ntziachristos, B. Chance, and A. G. Yodh, "Three-dimensional diffuse optical tomography in the parallel plane transmission geometry: Evaluation of a hybrid frequency domain/continuous wave clinical system for breast imaging," Med. Phys. **30**, 235–247 (2003).
[12]See supplementary material at http://dx.doi.org/10.1119/1.4739924 for an explanatory movie and NXT-G codes.
[13]Thorlabs homepage, <www.thorlabs.com/>, accessed April 2012.
[14]HiTechnic homepage, <http://www.hitechnic.com/>, accessed April 2012.
[15]BBraun homepage, <http://www.bbraun.com/>, accessed April 2012.
[16]Joves i Ciència de Catalunya homepage, <http://jovesiciencia.catalunyacaixa.es/>, accessed April 2012.